



A search for time dependent neutrino emission from microquasars with the ANTARES telescope



S. Adrián-Martínez^a, A. Albert^b, M. André^c, M. Anghinolfi^d, G. Anton^e, M. Ardid^a, T. Astraatmadja^{f,g}, J.-J. Aubert^h, B. Baretⁱ, J. Barrios^j, S. Basa^k, V. Bertin^h, S. Biagi^{l,m}, C. Bigongiari^j, C. Bogazzi^f, B. Bouhouⁱ, M.C. Bouwhuis^f, J. Brunner^h, J. Busto^h, A. Capone^{n,o}, L. Caramete^p, C. Cârloganu^q, J. Carr^h, S. Cecchini^l, Z. Charif^h, P. Charvis^r, T. Chiarusi^l, M. Circella^s, R. Coniglione^t, L. Core^h, H. Costantini^h, P. Coyle^h, A. Creusotⁱ, G. De Rosa^{u,v}, I. Dekeyser^{w,x}, A. Deschamps^r, G. De Bonis^{n,o}, C. Distefano^t, C. Donzaud^{i,y}, D. Dornic^h, Q. Dorosti^z, D. Drouhin^b, A. Dumas^q, T. Eberl^e, D. Elsässer^{aa}, U. Emanuele^j, A. Enzenhöfer^e, J.-P. Ernenwein^h, S. Escoffier^h, K. Fehn^e, I. Felis^a, P. Fermani^{n,o}, F. Folger^e, L.A. Fusco^{l,m}, S. Galatà^{i,*}, P. Gay^q, S. Geißelsöder^e, K. Geyer^e, V. Giordano^{ab}, A. Gleixner^e, J.P. Gómez-González^j, K. Graf^e, G. Guillard^q, H. van Haren^{ac}, A.J. Heijboer^f, Y. Hello^r, J.J. Hernández-Rey^j, B. Herold^e, J. Hößl^e, J. Hofestädt^e, C.W. James^e, M. de Jong^{f,g}, M. Kadler^{aa}, O. Kalekin^e, A. Kappes^e, U. Katz^e, P. Kooijman^{f,ad,ae}, A. Kouchnerⁱ, I. Kreykenbohm^{af}, V. Kulikovskiy^{ag,d}, R. Lahmann^e, E. Lambard^h, G. Lambard^j, G. Larosa^a, D. Lattuada^t, D. Lefèvre^{w,x}, E. Leonora^{ab,ah}, H. Loehner^z, S. Loucatos^{ai,i}, S. Mangano^j, M. Marcelin^k, A. Margiotta^{l,m}, J.A. Martínez-Mora^a, S. Martini^{w,x}, A. Mathieu^h, T. Michael^f, P. Migliozzi^u, T. Montaruli^{s,aj}, C. Müller^{af}, M. Neff^e, E. Nezri^k, D. Palioselitis^f, G.E. Pāvālaš^p, C. Perrina^{n,o}, P. Piattelli^t, V. Popa^p, T. Pradier^{ak}, C. Racca^b, G. Riccobene^t, R. Richter^e, C. Rivièrè^h, A. Robert^{w,x}, K. Roensch^e, A. Rostovtsev^{al}, M. Saldaña^a, D.F.E. Samtleben^{f,g}, A. Sánchez-Losa^j, M. Sanguineti^{d,am}, P. Sapienza^t, J. Schmid^e, J. Schnabel^e, S. Schulte^f, F. Schüssler^{ai}, T. Seitz^e, C. Sieger^e, A. Spies^e, M. Spurio^{l,m}, J.J.M. Steijger^f, T. Stolarczyk^{ai}, M. Taiuti^{d,am}, C. Tamburini^{w,x}, Y. Tayalati^{an}, A. Trovato^t, B. Vallage^{ai,i}, C. Vallée^h, V. Van Elewyckⁱ, P. Vernin^{ai}, E. Visser^f, D. Vivolo^{u,v}, S. Wagner^e, J. Wilms^{af}, E. de Wolf^{f,ae}, K. Yatkin^h, H. Yepes^j, J.D. Zornoza^j, J. Zúñiga^j

^a Institut d'Investigació per a la Gestió Integrada de les Zones Costaneres (IGIC), Universitat Politècnica de València, C/ Paranimf 1, 46730 Gandia, Spain

^b GRPHE – Université de Haute Alsace, Institut universitaire de technologie de Colmar, 34 rue du Grillenbreit, BP 50568, 68008 Colmar, France

^c Technical University of Catalonia, Laboratory of Applied Bioacoustics, Rambla Exposició, 08800 Vilanova i la Geltrú, Barcelona, Spain

^d INFN – Sezione di Genova, Via Dodecaneso 33, 16146 Genova, Italy

^e Friedrich-Alexander-Universität Erlangen-Nürnberg, Erlangen Centre for Astroparticle Physics, Erwin-Rommel-Str. 1, 91058 Erlangen, Germany

^f Nikhef, Science Park, Amsterdam, The Netherlands

^g Huygens–Kamerlingh Onnes Laboratorium, Universiteit Leiden, The Netherlands

^h CPPM, Aix-Marseille Université, CNRS/IN2P3, Marseille, France

ⁱ APC, Université Paris Diderot, CNRS/IN2P3, CEA/IRFU, Observatoire de Paris, Sorbonne Paris Cité, 75205 Paris, France

^j IFIC – Instituto de Física Corpuscular, Edificios Investigación de Paterna, CSIC – Universitat de València, Apdo. de Correos 22085, 46071 Valencia, Spain

^k LAM – Laboratoire d'Astrophysique de Marseille, Pôle de l'Étoile Site de Château-Gombert, rue Frédéric Joliot-Curie 38, 13388 Marseille Cedex 13, France

^l INFN – Sezione di Bologna, Viale Berti-Pichat 6/2, 40127 Bologna, Italy

^m Dipartimento di Fisica dell'Università, Viale Berti Pichat 6/2, 40127 Bologna, Italy

ⁿ INFN – Sezione di Roma, P.le Aldo Moro 2, 00185 Roma, Italy

^o Dipartimento di Fisica dell'Università La Sapienza, P.le Aldo Moro 2, 00185 Roma, Italy

^p Institute for Space Science, RO-077125 Bucharest, Măgurele, Romania

^q Laboratoire de Physique Corpusculaire, Clermont Université, Université Blaise Pascal, CNRS/IN2P3, BP 10448, F-63000 Clermont-Ferrand, France

^r Géoazur, Université Nice Sophia-Antipolis, CNRS/INSU, IRD, Observatoire de la Côte d'Azur, Sophia Antipolis, France

^s INFN – Sezione di Bari, Via E. Orabona 4, 70126 Bari, Italy

^t INFN – Laboratori Nazionali del Sud (LNS), Via S. Sofia 62, 95123 Catania, Italy

^u INFN – Sezione di Napoli, Via Cintia 80126, Napoli, Italy

^v Dipartimento di Fisica dell'Università Federico II di Napoli, Via Cintia 80126, Napoli, Italy

^w Mediterranean Institute of Oceanography (MIO), Aix-Marseille University, 13288, Marseille Cedex 9, France

^x Université du Sud Toulon-Var, CNRS-INSU/IRD U.M. 110, 83957, La Garde Cedex, France

^y Univ. Paris-Sud, 91405 Orsay Cedex, France

^z Kernfysisch Versneller Instituut (KVI), University of Groningen, Zernikelaan 25, 9747 AA Groningen, The Netherlands

^{aa} Institut für Theoretische Physik und Astrophysik, Universität Würzburg, Emil-Fischer Str. 31, 97074 Würzburg, Germany

^{ab} INFN – Sezione di Catania, Viale Andrea Doria 6, 95125 Catania, Italy

^{ac} Royal Netherlands Institute for Sea Research (NIOZ), Landsdiep 4, 1797 SZ 't Horntje (Texel), The Netherlands

^{ad} Universiteit Utrecht, Faculteit Betawetenschappen, Princetonplein 5, 3584 CC Utrecht, The Netherlands

^{ae} Universiteit van Amsterdam, Instituut voor Hoge-Energie Fysica, Science Park 105, 1098 XG, Amsterdam, The Netherlands

^{af} Dr. Remeis-Sternwarte and ECAP, Universität Erlangen-Nürnberg, Sternwartstr. 7, 96049 Bamberg, Germany

^{ag} Moscow State University, Skobel'syn Institute of Nuclear Physics, Leninskie gory, 119991 Moscow, Russia

^{ah} Dipartimento di Fisica ed Astronomia dell'Università, Viale Andrea Doria 6, 95125, Catania, Italy

^{ai} Direction des Sciences de la Matière, Institut de recherche sur les lois fondamentales de l'Univers, Service de Physique des Particules, CEA Saclay, 91191 Gif-sur-Yvette Cedex, France

^{aj} Département de Physique Nucléaire et Corpusculaire, Université de Genève, 1211, Geneva, Switzerland

^{ak} IPHC – Institut Pluridisciplinaire Hubert Curien, Université de Strasbourg et CNRS/IN2P3, 23 rue du Loess, BP 28, 67037 Strasbourg Cedex 2, France

^{al} ITEP – Institute for Theoretical and Experimental Physics, B. Chermushkinskaya 25, 117218 Moscow, Russia

^{am} Dipartimento di Fisica dell'Università, Via Dodecaneso 33, 16146 Genova, Italy

^{an} University Mohammed I, Laboratory of Physics of Matter and Radiations, B.P. 717, Oujda 6000, Morocco

ARTICLE INFO

Article history:

Received 4 March 2014

Accepted 9 June 2014

Available online xxxx

ABSTRACT

Results are presented on a search for neutrino emission from a sample of six microquasars, based on the data collected by the ANTARES neutrino telescope between 2007 and 2010. By means of appropriate time cuts, the neutrino search has been restricted to the periods when the acceleration of relativistic jets was taking place at the microquasars under study. The time cuts have been chosen using the information from the X-ray telescopes RXTE/ASM and Swift/BAT, and, in one case, the gamma-ray telescope Fermi/LAT. No statistically significant excess has been observed, thus upper limits on the neutrino fluences have been derived and compared to the predictions by models. Constraints have been put on the ratio of proton to electron luminosity in the jets.

© 2014 Elsevier B.V. All rights reserved.

1. Introduction

Microquasars are galactic X-ray binary systems exhibiting relativistic jets (Mirabel and Rodríguez, 1994) and are considered in some models to be a possible source of high energy (>100 GeV) neutrinos (Levinson and Waxman, 2001; Romero et al., 2003). The composition of the jets and in particular their baryonic content is still an open issue and is a key point for the expectations on the flux of neutrinos. Evidence for a baryonic content has been found only in the jets of the microquasars SS 433 and 4U 1630-47, witnessed by the observation of both blue and red Doppler shifted ionisation lines of heavy elements (Marshall et al., 2002; Díaz Trigo et al., 2013). Further observations have also indicated reheating (in situ acceleration) of the baryonic component at parsec scales in the jets of SS 433 (Migliari et al., 2002). Some hints in favour of a significant baryonic content in the outflow of the microquasar Cyg X-1 have been inferred using knowledge of the energetics of its jets: the observation of a radio-emitting large structure in the interstellar medium of Cyg X-1 has allowed the energy output of the jets to be constrained within the interval 10^{36} – 10^{37} erg s⁻¹ (Gallo et al., 2005), which is two orders of magnitude larger than the estimates based on the jet's flat radio spectrum (Fender et al., 2000). This excess of energy may be ascribed, among other things, to a population of cold baryons carried in the relativistic flow (Heinz, 2006). The observation of an X-ray emission from the parsec-scale jets of the microquasars XTE J1550-564 and H1743-322 with *Chandra* may imply the presence of ~ 10 TeV electrons, which would be most likely accelerated by shocks in the propagating plasma (Corbel et al., 2002, 2005).

If baryons were actually contained in microquasar jets and a dissipation mechanism allowed them to be accelerated to very

high energies, e.g. through diffusive shock acceleration, synchrotron emission from the electrons may provide the required opacity to photo-meson production and high energy neutrinos may be produced (Levinson and Waxman, 2001; Distefano et al., 2002). In microquasars harbouring an early type, massive ($\gtrsim 10M_{\odot}$) companion star, neutrinos may be generated by the interaction of the relativistic baryons in the jets with the ions from the stellar wind (Romero et al., 2003). The detection of high energy neutrinos from microquasars would thus give important clues about the composition of microquasar jets and about the physics taking place in the extreme environments close to black holes or neutron stars, and identify microquasars as one of the sources of the galactic component of cosmic rays.

This paper presents a search for neutrino emission from microquasars with the ANTARES detector. In order to maximise the signal to noise ratio, the atmospheric neutrino background is reduced by restricting the data to the times in which jet acceleration is supposed to take place at the sources under study. A multiwavelength approach using X-ray and gamma ray data is applied in order to select the outbursting periods. In Section 2, the ANTARES detector and the data set used in this analysis are described. The selected sources and the criteria adopted to define the time cuts for the neutrino search are presented in Section 3. In Section 4, the statistical method adopted to analyse the data is presented and the results are derived. Conclusions are drawn in Section 5.

2. ANTARES

The ANTARES neutrino telescope is an underwater detector optimised to detect neutrinos with energies above 100 GeV (Adrián-Martínez et al., 2011; Aguilar et al., 2011b). High energy neutrinos interacting with the matter surrounding the detector produce relativistic charged particles that induce the emission of Cherenkov light. Among neutrino flavours, muon neutrinos are

* Corresponding author.

the favoured probe for astrophysics, since muons' range in water reaches up to several kilometres at the energies of interest for ANTARES, thus allowing a more precise reconstruction of their direction and an effective volume higher than the instrumented volume.

The detector consists of an array of 885 photomultiplier tubes (PMTs) located in the Mediterranean Sea at a depth of 2475 m, 40 km offshore from the southern coast of France. It is composed of 12 detection lines each hosting 75 optical modules (OMs, Amram et al., 2002), arranged in 25 storeys, with 3 OMs on each storey. The OMs are inclined towards the bottom by 45° to favour the detection of upward-going tracks. The storeys are equally spaced along the lines by 14.5 m. The spacing between the lines is approximately 60 m.

The light signals detected by the OMs, the “hits”, are digitised by electronics boards placed on each storey and then sent to a PC farm onshore that performs the filtering of the data (Aguilar et al., 2007). The data filtering algorithm is based on the occurrence of “L1 hits”, i.e., coincidences of two hits within a single storey, or single hits with collected charge higher than 3 photoelectrons. The algorithm selects the events containing at least five causally connected L1 hits or a local cluster of neighbouring L1 hits. An appropriate time calibration procedure is applied to the arrival time of the light signals (Aguilar et al., 2011a), whereas a positioning system takes care of recording the displacement of the lines, due to the sea currents (Adrián-Martínez et al., 2012a). A detailed description of the ANTARES detector and its calibration procedures can be found in (Ageron et al., 2011, and references therein).

The ANTARES detector started taking physics data in January 2007, when it was composed of only five detection lines. It was upgraded to ten detection lines in December 2007 and was completed in May 2008 with its twelve-line configuration. This paper describes an analysis of the ANTARES data collected between January 2007 and the end of 2010.

The reconstruction of muon tracks is performed by means of a multi-step procedure whose final result is provided by a maximum likelihood fit (Adrián-Martínez et al., 2012b). The quality parameter of the reconstructed tracks, here referred to as Λ , is defined on the basis of the maximised likelihood. The algorithm also provides an estimate of the angular uncertainty of the reconstructed direction event-by-event, here referred to as β . Only tracks with $\beta < 1^\circ$ are selected for the analysis. The response of the detector and the performances of the reconstruction algorithm are estimated by means of Monte Carlo simulations. Atmospheric neutrinos, which represent an irreducible background, are simulated according to the flux obtained by Agrawal et al. (1996). The flux of atmospheric muons reaching the detector from above is simulated with the code MUPAGE (Carminati et al., 2008).

Due to the intense flux of downgoing atmospheric muons, only tracks reconstructed as upgoing are selected as neutrino candidates. Nevertheless, a fraction of atmospheric muons can be misreconstructed as upgoing and contaminate the neutrino sample. These background tracks are reconstructed with a low quality and can be discarded by applying a suitable cut on Λ . Two cuts on Λ are used in this analysis: $\Lambda > -5.2$ and $\Lambda > -5.4$. These cut values result from the optimisation procedure described in Section 4, and lead to a contamination from atmospheric muons of 13% and 42%, respectively. Fig. 1 shows a comparison between data and Monte Carlo of the distribution of the reconstruction quality Λ for upgoing tracks with angular uncertainty $\beta < 1^\circ$.

The angular resolution of ANTARES is also estimated using Monte Carlo simulations and depends on the assumed neutrino spectrum. The cumulative distribution of the angular error of the reconstructed neutrinos is shown in Fig. 2 for two different quality cuts and a spectrum $\propto E_\nu^{-2}$ and $\propto E_\nu^{-2} \exp(-\sqrt{E_\nu}/100 \text{ TeV})$. The

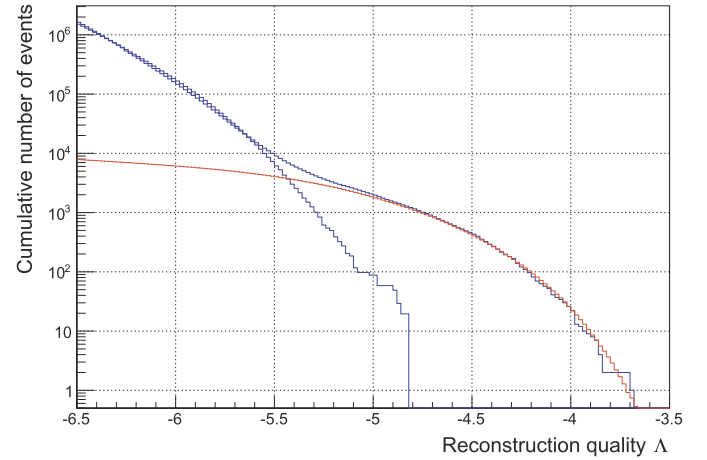


Fig. 1. Cumulative distribution of the track reconstruction quality parameter Λ for the data (black) and for the simulated atmospheric muons (blue) and neutrinos (red), for upgoing tracks with $\beta < 1^\circ$. (For interpretation of the references to colour in this figure legend, the reader is referred to the web version of this article.)

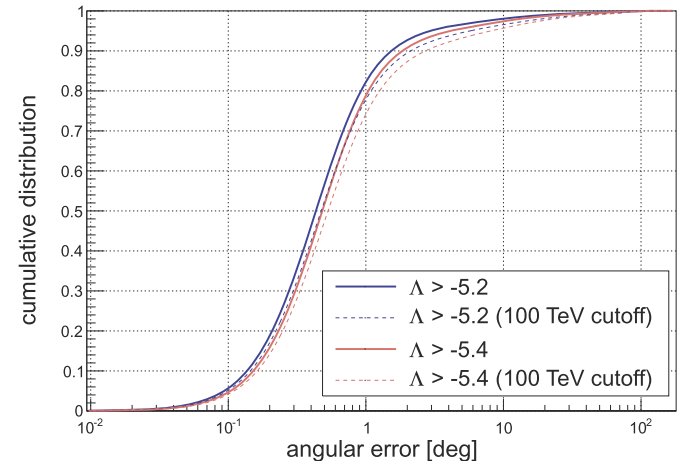


Fig. 2. Cumulative distribution of the angular error of the reconstruction algorithm for two different quality cuts and a neutrino source with an energy spectrum $\propto E_\nu^{-2}$ (solid) and $\propto E_\nu^{-2} \exp(-\sqrt{E_\nu}/100 \text{ TeV})$ (dashed).

median angular resolution for an E_ν^{-2} spectrum is $0.46 \pm 0.10 \text{ deg}$ (Adrián-Martínez et al., 2012b), using a cut $\Lambda > -5.2$.

3. Selection of flaring time periods

Among the sources listed as microquasars in the catalogues of X-ray binaries (Liu et al., 2006, 2007) and visible by ANTARES, those showing an outburst that could be associated with the acceleration of relativistic jets are selected for this analysis. The selected sources, ordered by increasing declination, are: CirX-1, GX 339-4, H1743-322, IGRJ17091-3624, Cyg X-1 and Cyg X-3. To maximise the detection probability, the search for coincident neutrino events is restricted to microquasar flaring time periods. The selection of flaring periods is carried out by taking into account the multi-wavelength behaviour of each of the selected microquasars, using information from X-ray or gamma-ray instruments.

For all the microquasars considered in this paper, except Cyg X-3, the time selection is based on their X-ray behaviour. When the procedure involves the selection of X-ray outbursts in the daily averaged X-ray light curves of RXTE/ASM¹ (1.2–12 keV) or

¹ RXTE/ASM data are taken from <http://xte.mit.edu/asmlc/>.

Swift/BAT² (15–50 keV), a dedicated outburst selection algorithm is adopted.

To infer the onset of an X-ray outburst, a Gaussian fit is performed to the distribution of the X-ray rates to calculate the baseline rate, $\langle r \rangle$, and its standard deviation, $\sigma_{\langle r \rangle}$. The fit is iterated twice within the interval $\langle r \rangle_{-2\sigma_{\langle r \rangle}}^{+\sigma_{\langle r \rangle}}$, to reduce the contribution from the bursting region. The light curve is then scanned, looking for a rate measurement \tilde{r} satisfying the condition $\tilde{r} - 3\sigma_{\tilde{r}} > \langle r \rangle + 3\sigma_{\langle r \rangle}$, where $\sigma_{\tilde{r}}$ is the error on the single rate measurement. Once such a measurement is found, all the following and preceding measurements for which $\tilde{r} - \sigma_{\tilde{r}} > \langle r \rangle + 3\sigma_{\langle r \rangle}$ are selected. At least two consecutive measurements are required for the selection to take place. In the case of Cyg X-3 the time selection is based on the Fermi/LAT gamma-ray light curve, hence a slightly different procedure is used to select the outbursts, as described in Section 3.3.

As the increase of the X-ray flux alone is not generally sufficient to ensure the onset of a relativistic jet, additional time selection criteria, customised for the features of each microquasar under study, are applied and are described in the following.

3.1. Black hole binaries

Four of the microquasars considered in this analysis are black hole candidates or confirmed black hole binaries. The time evolution of X-ray outbursts in this type of source is known to follow a specific pattern in the intensity and spectrum of the X-ray flux (see Belloni, 2010, for a review). The beginning of an outburst is characterised by a power-law energy spectrum with photon index ~ 1.7 , known as the *hard state*, during which a steady jet is observed with Lorentz factor ~ 2 . This is followed by an X-ray state in which the hard power law component is almost suppressed in favour of a soft thermal component with temperature ~ 1 keV, referred to as the *soft state*, during which the radio jet is suppressed and the disk emission is dominant. The transition between these two canonical states, which are rather stable and can last several weeks, takes place through two intermediate states, the hard and soft intermediate states (HIMS and SIMS, respectively), both characterised by spectral features between the hard and soft states. These transitions occur on time scales of hours/days and are often associated with discrete-ejection observed in radio wavelengths whose Lorentz factor is thought to be higher than that observed during the hard state (Fender et al., 2004b, 2009).

The time selection for the following sources is based entirely on their X-ray behaviour, by taking into account the disk-jet coupling just described. Only periods of hard X-ray states and state transitions are selected, since they correspond to phases where relativistic jets are present, and therefore neutrino emission is expected. Also, both states are considered separately for the subsequent neutrino search.

3.1.1. GX339-4

GX339-4 is a galactic black hole binary system (Hynes et al., 2003; Zdziarski et al., 2004) that has undergone two major outbursts between 2007 and 2010, both featuring a hard to soft transition, and some fainter ones (see Fig. 3).

The hard states have been selected as outbursts in the Swift/BAT daily averaged light curve, using the procedure described at the beginning of this section. The times of the transitions as well as of the onset of the soft state are estimated using X-ray spectral observations, and are used to define the end of the hard state.

At the beginning of 2007 the source was already in outburst. From a detailed study of the spectral time evolution of GX339-4

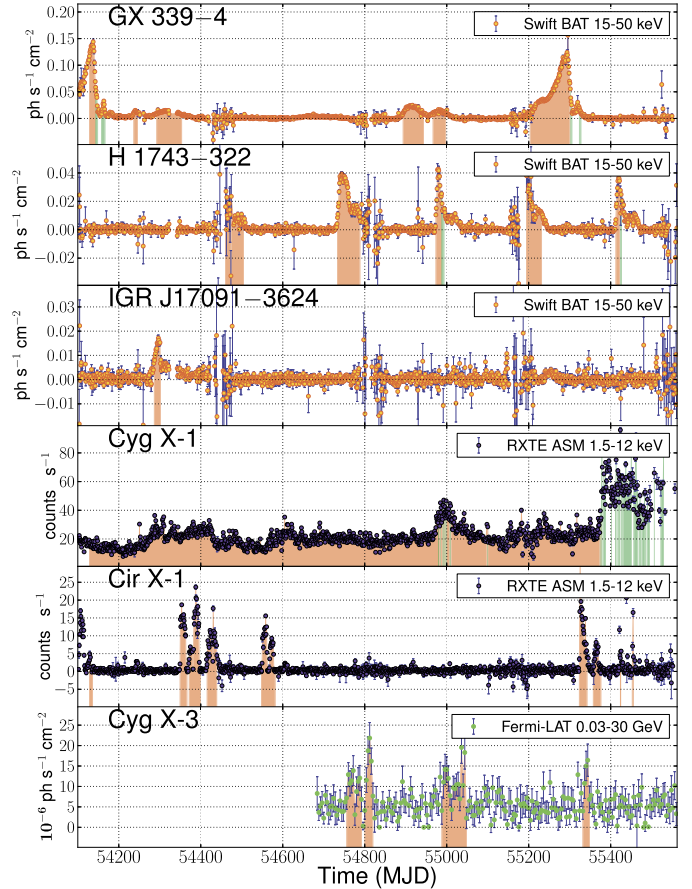


Fig. 3. X-ray and gamma-ray light curves (Swift/BAT in red, RXTE/ASM in blue and Fermi/LAT in green) used for the selection of the flaring times. The shaded areas represent the times selected for the analysis. The red and green areas in the light curves of GX339-4, H1743-322 and Cyg X-1 correspond to hard states and state transitions, respectively. (For interpretation of the references to colour in this figure legend, the reader is referred to the web version of this article.)

during this outburst, the transition from the HIMS to the SIMS is observed around MJD 54145.5, and then again around MJD 54160 and MJD 54164 (Motta et al., 2009). A similar outburst was again observed in the first half of 2010. The decay phase of this outburst and the subsequent transition to softer states has been followed by RXTE/PCA pointed observations by Belloni et al. (2010), who locate the transition from the HIMS to the SIMS at around MJD 55304, after which the source was observed undergoing a transition to the soft state and then to the SIMS until MJD 55316. On MJD 55320 the X-ray spectrum was compatible with the source being in the HIMS again (Motta et al., 2010), but the subsequent transition was not observed, though from the light curves and the similarity with the 2007 outburst, the time at which it occurred can be estimated to be around MJD 55324. A time window of 5 days centred at the estimated time of the state transitions is selected for the neutrino search. Its start time coincides with the end of the hard state period preceding it.

3.1.2. H1743-322

For the black hole candidate H1743-322 (McClintock et al., 2009) the same selection procedure used for GX339-4 is adopted. Between 2007 and 2010, H1743-322 has undergone five outbursts (Fig. 3).

The outburst that occurred at the end of 2008 has been classified as a failed outburst (Capitanio et al., 2009), since the source remained between the hard state and the HIMS without reaching the soft state or the SIMS. The subsequent outburst that occurred

² Swift/BAT data are taken from <http://heasarc.nasa.gov/docs/swift/results/transients/>.

in 2009 featured, after the onset of the hard state, a HIMS → SIMS transition at MJD 54990 (Chen et al., 2010), which is included in a time window of ± 2.5 days for the transitional phase search. The evolution of the outburst detected in 2010 is described in (Nakahira et al., 2010, and references therein). A HIMS → SIMS transition is observed around MJD 55424.5, after which the source stays in the soft state until quiescence. Two more outbursts were observed while the source was close to the Sun and thus received a poor coverage by X-ray telescopes. The first was detected around MJD 54453 and lasted until MJD 54504 (Kalemci et al., 2007; Jonker et al., 2010). The second was detected around MJD 55191 until MJD 55237 (Yamaoka et al., 2009, and references therein). These are also included in the analysis as hard states, since it is not known whether state transitions have taken place.

3.1.3. IGRJ17091-3624

For the black hole candidate IGRJ17091-3624 (Pandey et al., 2006) a short outburst was observed in the Swift/BAT daily light curve between MJD 54286 and MJD 54301 (Fig. 3), which has been selected for the analysis. Swift/XRT observations during that period confirmed a hardening of the X-ray spectrum (Kennea and Capitanio, 2007).

3.1.4. CygX-1

The time selection for the black hole binary CygX-1 (Bowyer et al., 1965; Webster and Murdin, 1972; Stirling et al., 2001) is performed differently to the black hole binaries or black hole candidates discussed previously. By comparing simultaneous RXTE/PCA and RXTE/ASM data on a long term monitoring of CygX-1, Grinberg et al. (2013) have shown how to perform an almost exact mapping of the X-ray spectral state on the basis of the sole RXTE/ASM flux and hardness. This mapping is used in order to define the onset of a hard or intermediate state for this source. The results of this selection are shown in Fig. 3.

3.2. CirX-1

CirX-1 is the only confirmed neutron star microquasar considered in this analysis. It has an orbital period of 16.6 days (Kaluzienski et al., 1976) and undergoes regular radio flares with the same period, interpreted as enhanced accretion near periastron passage in a highly eccentric orbit (Murdin et al., 1980). A high angular resolution monitoring campaign in the radio, conducted with e-VLBI in 2009, has confirmed this behaviour, observing an enhanced radio emission between orbital phase 0.09 and 0.21 (Moín et al., 2011), although these measurements were taken during a period of very low activity in both radio and X-rays. Simultaneous radio and X-ray observations have shown that an increased accretion rate, in the form of an X-ray outburst, is followed by the acceleration of relativistic jets, observed as a brightening of the radio core of the source, followed by the brightening of the arc-second scale radio structure surrounding the core (Fender et al., 2004a).

This source has undergone several X-ray outburst events between 2007 and 2010, better visible in the soft X-rays (Fig. 3), that are included in the analysis using the procedure described at the beginning of this section applied to the daily averaged light curves of RXTE/ASM. If sufficiently close in time, i.e. within 4 days, the selected periods are extended, forward or backward, in order to include the expected radio flare at superior conjunction.

3.3. CygX-3

CygX-3 is a high-mass binary (van Kerkwijk et al., 1992; Parsignault et al., 1972) in which the nature of the compact object has not yet been identified. It has been observed emitting

high energy gamma-rays by both AGILE (Tavani et al., 2009) and Fermi/LAT (Abdo et al., 2009), in association with its ultra soft X-ray states which in turn are related to giant radio outbursts. Thus the time selection for this source is based on its behaviour in gamma-rays.

The gamma-ray data between 30 MeV and 30 GeV from Fermi/LAT³ are analysed using the procedure described by Abdo et al. (2009).⁴ The light curve is calculated in time bins of four days and is shown in Fig. 3. The selection of gamma-ray flares is performed in the same fashion as the one described for the X-rays at the beginning of this section, with some modifications due to the different nature of the data. Namely, a Gaussian fit is performed on the distribution of the gamma-ray rate r , to calculate its mean value $\langle r \rangle$ and its standard deviation $\sigma_{(r)}$. All the times corresponding to a flux measurement \tilde{r} for which $\tilde{r} - \sigma_{\tilde{r}} > \langle r \rangle$, where $\sigma_{\tilde{r}}$ is the error on the flux measurement, are then included in the analysis within a time window of 4 days, which is the binning used to produce the light curve. The obtained time windows are extended by 5 days before and after, to take into account the possible time lags between the gamma-ray emission and the development of the jets (Williams et al., 2011). The results of this selection are shown in Fig. 3.

4. Search for coincident neutrino events

4.1. Statistical method

The ANTARES data collected between 2007 and 2010, corresponding to 813 days of livetime, are analysed to search for neutrino events around the selected sources, in coincidence with the time periods defined in the previous section and listed in Table 1. The statistical method adopted to infer the presence of a signal on top of the atmospheric neutrino background, or alternatively set upper limits on the neutrino flux is an unbinned method based on a likelihood ratio test statistic. The likelihood is defined as:

$$\log(\mathcal{L}) = \sum_{i=1}^{n_{\text{tot}}} \log[n_{\text{sig}}S(\alpha_i) + n_{\text{tot}}\mathcal{B}(\theta_i)] - n_{\text{tot}}, \quad (1)$$

where n_{tot} is the total number of neutrino events detected during the flaring periods and while the source was visible by ANTARES (i.e., below the horizon). In Eq (1), S is the point spread function (PSF), α_i is the angular distance of the event i from the position of the source, \mathcal{B} is the distribution of background events as a function of the zenith angle θ_i , and both S and \mathcal{B} are normalised to 1. A spectrum of the form $dN/dE_\nu = \phi E_\nu^{-2} \text{ GeV cm}^{-2} \text{ s}^{-1}$ is used to optimise the search and to calculate the upper limits of the neutrino fluences, whereas a customised spectral shape is used to compare the results with model predictions (Section 4.2). The normalisation constant ϕ is the quantity to be measured or upon which upper limits are set. The result of each search is based on the value assumed by the test statistic variable ξ , which is defined as the logarithm of the ratio between the likelihoods calculated under the hypotheses of background plus signal and background-only:

$$\xi = \max\{\log \mathcal{L}(n_{\text{sig}})\} - \log \mathcal{L}(n_{\text{sig}} = 0). \quad (2)$$

Monte Carlo pseudo experiments are generated to compute the distributions of ξ under the background only and background plus signal hypotheses. Each pseudo experiment simulates the number

³ Fermi/LAT data have been retrieved from the web page <http://fermi.gsfc.nasa.gov/cgi-bin/ssc/LAT/LATDataQuery.cgi>.

⁴ This analysis has been performed using HEASOFT v6.11, ScienceTools v9r23p1 and the response function P6_V1_DIFFUSE.

Table 1
Candidate microquasars and selected periods.

Source name	Selected periods (MJD)
Cir X-1	54128–54136, 54349–54367, 54371–54400, 54415–54442, 54547–54582, 55323–55343, 55357–55375, 55421–55426, 55452–55458
GX 339-4 (hard state)	54128–54143, 54236–54246, 54292–54354, 54893–54944, 54966–54998, 55203–55301
GX 339-4 (transition)	54143–54148, 54157.5–54166.5, 55301–55306, 55323–55328
H1743-322 (hard state)	54453–54504, 54733–54789, 54973–54987.5, 55191–55237, 55412–55422
H1743-322 (transition)	54987.5–54992.5, 55422–55427
IGRJ17091-3624 (hard state)	54286–54301
Cyg X-1 (hard state)	54128–54979, 54980–54984, 54985–54990, 54991–54992, 54993–54995, 54997–54998, 54999–55007, 55008–55009, 55010–55099, 55100–55374, 55375–55377
Cyg X-1 (transition)	54979–54980, 54984–54985, 54990–54991, 54992–54993, 54995–54997, 54998–54999, 55007–55008, 55009–55010, 55099–55100, 55374–55375, 55377–55379, 55381–55388, 55401–55402, 55411–55414, 55417–55418, 55419–55422, 55425–55429, 55430–55451, 55456–55467, 55470–55475, 55477–55483, 55484–55485, 55488–55492, 55494–55495, 55506–55507, 55522–55523, 55528–55530
Cyg X-3	54753–54795, 54797–54823, 54985–55051, 55329–55351

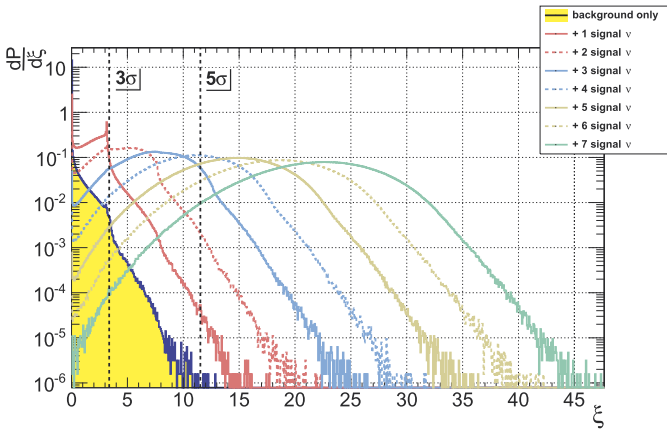


Fig. 4. Probability distribution of the test statistic variable issued from pseudo experiments for background only (solid histogram) and by adding from 1 up to 7 signal neutrinos around the source. The vertical dashed lines indicate the threshold values of ξ that lead to a 3σ and 5σ pre-trial rejection of the background only hypothesis. This plot corresponds to the case of GX 339-4 during hard states.

of neutrinos selected in the data. The simulated neutrino directions for the background events are randomly generated according to the zenith and azimuth distribution of the neutrinos selected in the whole ANTARES 2007–2010 data set. The conversion to celestial coordinates is done using the true time of the detected event. To simulate the presence of a signal, pseudo experiments are also generated by adding from one up to thirty neutrinos distributed around the source according to the ANTARES PSF. An example of the resulting distributions of the test statistic for background-only and background plus a fixed number of injected signals, $P(\xi|n_{\text{sig}})$, is shown in Fig. 4 for the case of GX 339-4 outbursts during hard states. The distribution of the test statistic for a mean number of signals $P(\xi|n_{\text{sig}})$ is calculated from a Poissonian convolution of the $P(\xi|n_{\text{sig}})$:

$$P(\xi|n_{\text{sig}}) = \sum_{n_{\text{sig}}} P(\xi|n_{\text{sig}}) \frac{\langle n_{\text{sig}} \rangle^{n_{\text{sig}}} e^{-\langle n_{\text{sig}} \rangle}}{n_{\text{sig}}!}, \quad (3)$$

and is used to construct the 90% confidence belts with the unified approach of Feldman and Cousins (1998). The conversion between $\langle n_{\text{sig}} \rangle$ and the normalisation of the neutrino flux ϕ is performed by means of Monte Carlo simulations. The average

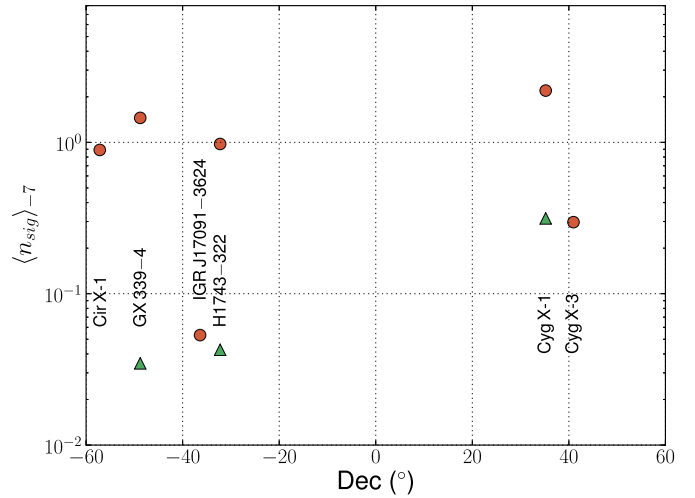


Fig. 5. Number of neutrino events expected by ANTARES from a source with an E_{ν}^{-2} spectrum and a flux normalisation of $10^{-7} \text{ GeV cm}^{-2} \text{ s}^{-1}$ when applying the time and quality cuts listed in Table 1 and Table 2, as a function of the source declination. The green triangles stand for black hole binary transitional states.

number of expected neutrino events $\langle n_{\text{sig}} \rangle_{-7}$ from the selected sources assuming an E_{ν}^{-2} spectrum and a flux normalisation $\phi_{-7} = 10^{-7} \text{ GeV cm}^{-2} \text{ s}^{-1}$ is shown in Fig. 5 as a function of the source declination. This quantity is used to convert the upper limits $\langle n_{\text{sig}} \rangle^{90\% \text{ CL}}$ to an upper limit on the flux normalisation $\phi^{90\% \text{ CL}}$ by a proportional scaling:

$$\phi^{90\% \text{ CL}} = \phi_{-7} \frac{\langle n_{\text{sig}} \rangle^{90\% \text{ CL}}}{\langle n_{\text{sig}} \rangle_{-7}}. \quad (4)$$

The quality cuts on Λ to be used in each neutrino search are optimised in order to minimise the flux needed for a 5σ discovery in 50% of pseudo experiments for an E_{ν}^{-2} spectrum, and are listed in Table 2. The optimisation is carried out only on the basis of the results of the pseudo experiments and while keeping the true neutrino directions in the data unknown.

4.2. Results

The above statistical method has been applied to calculate the ξ value of each neutrino search. The results are summarised in

Table 2

Summary of the results of the neutrino searches for the microquasars studied in this paper. The columns report the values of the adopted cut on the track reconstruction quality Δ , the test statistic ξ , the livetime of the search, the number of neutrinos selected in the whole sky during the selected periods and while the source was below the horizon, the distance of the closest of these neutrinos to the source, the 90% C.L. upper limit on the neutrino fluence $\mathcal{F}_\nu^{90\%CL}$ and on the energy flux of neutrinos $f_\nu^{90\%CL}$, respectively. The last two quantities are given supposing both an E_ν^{-2} and an $E_\nu^{-2} \exp(-\sqrt{E_\nu}/100 \text{ TeV})$ neutrino spectrum.

Source name	$\Delta >$	ξ	Livetime (days)	n_{tot}	Closest ν	$\mathcal{F}_\nu^{90\%CL}$ (GeV cm $^{-2}$)		$f_\nu^{90\%CL}$ (erg cm $^{-2}$ s $^{-1}$)	
						no cutoff	100 TeV cutoff	no cutoff	100 TeV cutoff
Cir X-1	-5.2	0	100.5	257	5.7°	16.8	9.1	3.11×10^{-9}	1.68×10^{-9}
GX 339-4 (HS)	-5.2	0	147.0	485	2.8°	10.9	9.3	1.37×10^{-9}	1.18×10^{-9}
GX 339-4 (TS)	-5.4	0	4.9	14	11°	19.4	16.6	7.34×10^{-8}	6.27×10^{-8}
H1743-322 (HS)	-5.2	0	83.6	444	4.6°	9.2	7.1	2.04×10^{-9}	1.58×10^{-9}
H1743-322 (TS)	-5.4	0	3.3	22	15.9°	10.2	7.7	5.71×10^{-8}	4.33×10^{-8}
I GRJ17091-3624	-5.4	0	8.5	40	12°	21.0	19.0	4.57×10^{-8}	4.15×10^{-8}
Cyg X-1 (HS)	-5.2	0	182.8	671	1.4°	9.4	29.3	9.57×10^{-10}	2.98×10^{-9}
Cyg X-1 (TS)	-5.4	0	18.5	117	6.4°	6.0	6.7	5.98×10^{-9}	6.75×10^{-9}
Cyg X-3	-5.4	0	16.6	144	6.9°	5.7	7.0	6.34×10^{-9}	7.83×10^{-9}

Table 3

Parameters used to calculate the neutrino flux expectations for the microquasars considered in this analysis using the formulation by Distefano et al. (2002). The columns report: the distance of the microquasar, the inclination angle of the jet with respect to the line of sight, the jet velocity, Lorentz factor and Doppler factor, the size of the radio emitting region in units of 10^{15} cm, the frequency of the radio observation and the corresponding measured flux density during an outburst. The last column reports the 90% confidence level upper limits on the ratio η_p/η_e resulting from the upper limits on the neutrino flux reported in Table 2 (100 TeV cutoff case).

Source name	D (kpc)	θ (deg)	β	Γ	δ	l_{15}	ν (GHz)	S_ν (mJy)	$\eta_{p,-1}^{-1} \eta_{e,-1}^{1/2} f_\nu^{th}$ (erg cm $^{-2}$ s $^{-1}$)	Reference	(η_p/η_e) u.l.
Cir X-1 (1)	7.8	10	0.92	2.55	4.17	1.17	8.4	200	2.37×10^{-10}	1, 2, 3, 4	7.1
Cir X-1 (2)	7.8	50	0.50	1.15	1.28	1.17	8.4	200	3.28×10^{-11}	1, 2, 3, 4	51.2
GX 339-4	8	50	0.87	2.0	1.12	0.60	8.6	20	5.25×10^{-12}	5, 6, 7, 8, 9	224.6
H1743-322	8.5	75.0	0.20	1.02	1.03	0.38	9.0	24	2.37×10^{-12}	10, 11	666.9
Cyg X-1	1.8	33	0.60	1.25	1.48	0.21	15.0	10	4.25×10^{-12}	12, 13, 14, 15	701.4
Cyg X-3	10	25.7	0.56	1.21	1.67	0.60	15.0	1000	1.60×10^{-10}	16, 17, 18	49

References: (1) Goss and Mebold (1977); (2) Jonker and Nelemans (2004); (3) Miller-Jones et al. (2012a); (4) Calvelo et al. (2010); (5) Zdziarski et al. (2004); (6) Shidatsu et al. (2011); (7) Casella et al. (2010); (8) Gallo et al. (2004); (9) Corbel et al. (2007); (10) Steiner et al. (2012); (11) Miller-Jones et al. (2012b); (12) Xiang et al. (2011); (13) Gies and Bolton (1986); (14) Stirling et al. (2001); (15) Fender et al. (2006); (16) Predehl et al. (2000); (17) Miller-Jones et al. (2004); (18) Williams et al. (2011).

Table 2. As none of the searches has produced a statistically significant neutrino excess above the expected background, the 90% confidence level upper limits on the flux normalisation $\phi^{90\%CL}$ of an E_ν^{-2} and an $E_\nu^{-2} \exp(-\sqrt{E_\nu}/100 \text{ TeV})$ spectrum are calculated. Systematic uncertainties of 15% on the angular resolution and 15% on the detector acceptance have been included in the upper limit calculations. These systematic errors have been constrained on the basis of a 30% uncertainty on the atmospheric neutrino flux as shown by Adrián-Martínez et al. (2012b). Also, a systematic uncertainty on the absolute orientation of the detector of ~ 0.1 deg has been taken into account (Adrián-Martínez et al., 2012a). The $\phi^{90\%CL}$ are used to obtain the upper limits of the neutrino fluences, i.e. the energy per unit area, as (in the case of an E_ν^{-2} spectrum):

$$\mathcal{F}_\nu^{90\%CL} = \phi^{90\%CL} \Delta T_{\text{search}} \int_{10^2 \text{ GeV}}^{10^8 \text{ GeV}} E_\nu \cdot E_\nu^{-2} dE_\nu, \quad (5)$$

where ΔT_{search} is the corresponding livetime of the search. The upper limits obtained on the fluence as well as those on the energy flux in neutrinos (calculated as $f_\nu^{90\%CL} = \mathcal{F}_\nu^{90\%CL} / \Delta T_{\text{search}}$) are reported in Table 2.

The neutrino flux predictions according to the model by Distefano et al. (2002) have been calculated using the latest measurements of the distance and of the jet parameters of the microquasars, and are reported in Table 3 together with the parameters used to compute them. For the microquasar Cir X-1 two possibilities for the jet inclination and Lorentz factor are considered, whereas no measurement is found to estimate the neutrino flux from IGRJ17091-3624. To account for muon neutrino disappearance due to neutrino oscillations, a factor of 0.5 is applied to the flux expectations, which was not included in Distefano et al. (2002). In the framework of Levinson and Waxman (2001) and Distefano et al. (2002), the neutrino flux prediction is linearly

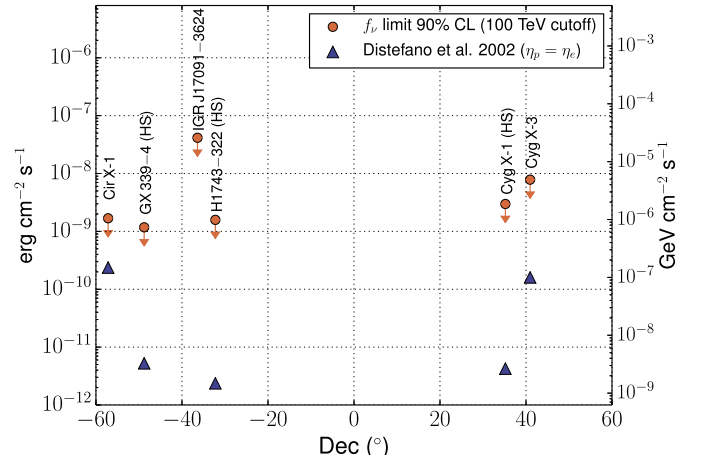


Fig. 6. Feldman–Cousins 90% confidence level upper limits on the energy flux in neutrinos f_ν obtained in this analysis considering a flux $\propto E^{-2} \exp(-\sqrt{E_\nu}/100 \text{ TeV})$ (circles), compared with the expectations by Distefano et al. (2002) in the case $\eta_p = \eta_e$ (triangles).

dependent on η_p/η_e , where η_p and η_e are the fraction of jet luminosity tapped to accelerate protons and electrons, respectively. In order to put constraints on the ratio η_p/η_e , the predictions are compared with the upper limits obtained under the hypothesis of a cutoff at 100 TeV in the neutrino flux, to take into account the limitation in the acceleration process included in the model. The resulting 90% confidence level upper limits on η_p/η_e are shown in Table 3. Fig. 6 shows the comparison between the upper limits on the energy flux in neutrinos and the model expectations obtained by setting $\eta_p = \eta_e = 0.1$. The latter case cannot be excluded for any of the sources.

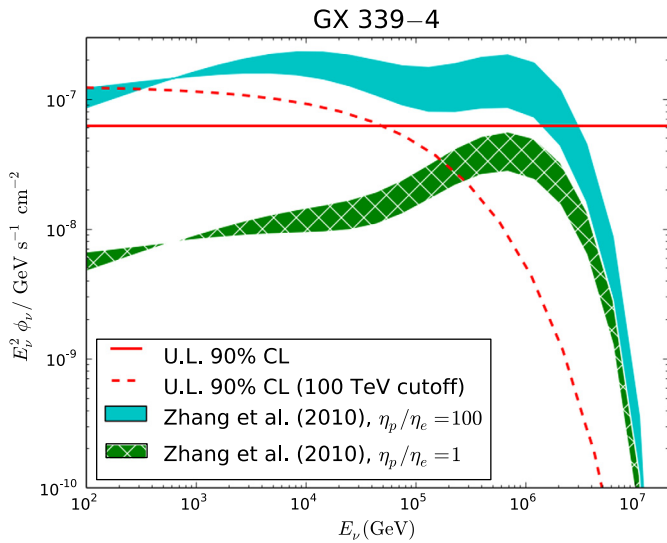


Fig. 7. Upper limits at 90% C.L. on the neutrino flux for GX 339-4 in both the hypotheses without and with the cutoff at 100 TeV, compared to the prediction by Zhang et al. (2010) for a spectral index of the injected particles $1.8 < \alpha < 2.0$ and the ratio η_p/η_e equal to 1 and 100, respectively.

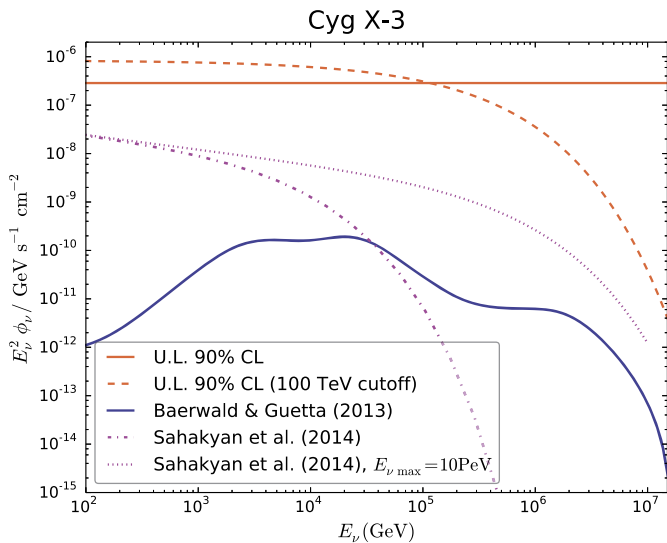


Fig. 8. Upper limits at 90% C.L. on the neutrino flux for Cyg X-3 in both the hypotheses without and with the cutoff at 100 TeV, compared to the predictions by Baerwald and Guetta (2013) and Sahakyan et al. (2014).

Zhang et al. (2010) have provided a calculation of the high-energy neutrino emission from GX 339-4 in the hypothesis that the primary spectrum of the injected particles in the jets has spectral indexes $\alpha = -1.8, -2.0$ and that the ratio η_p/η_e^5 is equal to 1 and 100, respectively. The comparison between our upper limits and the expectations by Zhang et al. (2010) is shown in Fig. 7. Our upper limit, in the case without cutoff, excludes the model for $\eta_p/\eta_e = 100$, whereas it is still above the expectations for $\eta_p/\eta_e = 1$. Fig. 8 shows the comparison between the neutrino flux expectations from Cyg X-3 provided by Baerwald and Guetta (2013) and Sahakyan et al. (2014), and the upper limits obtained in this analysis, which are above the model expectations.

5. Conclusions

This paper presents a search for neutrino emission from microquasars during outbursts with the data collected by the ANTARES telescope between 2007 and 2010. The search has been performed under the hypothesis that relativistic jets from microquasars contain baryons that interact during their acceleration or propagation, and time cuts have been chosen to isolate jet acceleration events. The searches did not result in a statistically significant excess above the expected background, thus the 90% C.L. upper limits on the neutrino fluences have been calculated. The predictions from the model by Distefano et al. (2002) have been computed and compared to our upper limits in order to constrain the ratio of proton to electron luminosity (η_p/η_e). For the microquasar Cir X-1, we obtain that $\eta_p/\eta_e < 7$ or < 50 , depending on the choice of the jet velocity and inclination angle. For the microquasar GX 339-4 we obtain that $\eta_p/\eta_e < 225$ when comparing to Distefano et al. (2002) expectations, whereas our result excludes the model by Zhang et al. (2010) in the case $\eta_p/\eta_e = 100$.

Additional ANTARES data will eventually improve the results obtained in this paper with the inclusion of new outbursts and extend the search to microquasars that remained quiescent between 2007 and 2010. Depending on the outburst intensity, duty cycle and on the jet parameters of the sources, the model expectations may rise to a level that is detectable by ANTARES or, in the longer term, by the forthcoming KM3NeT neutrino telescope (Adrián-Martínez et al., 2013).

Acknowledgments

The authors acknowledge the financial support of the funding agencies: Centre National de la Recherche Scientifique (CNRS), Commissariat à l'énergie atomique et aux énergies alternatives (CEA), Agence Nationale de la Recherche (ANR), Commission Européenne (FEDER fund and Marie Curie Program), Région Alsace (contract CPER), Région Provence-Alpes-Côte d'Azur, Département du Var and Ville de La Seyne-sur-Mer, France; Bundesministerium für Bildung und Forschung (BMBF), Germany; Istituto Nazionale di Fisica Nucleare (INFN), Italy; Stichting voor Fundamenteel Onderzoek der Materie (FOM), Nederlandse Organisatie voor Wetenschappelijk Onderzoek (NWO), the Netherlands; Council of the President of the Russian Federation for young scientists and leading scientific schools supporting grants, Russia; National Authority for Scientific Research (ANCS), Romania; Ministerio de Ciencia e Innovación (MICINN), Prometeo of Generalitat Valenciana and MultiDark, Spain; Agence de l'Oriental and CNRST, Morocco. We also acknowledge the technical support of Ifremer, AIM and Foselev Marine for the sea operation and the CC-IN2P3 for the computing facilities.

References

- Abdo, A.A., et al., 2009. *Science* 326, 1512.
- Adrián-Martínez, S., et al., 2011. *Astrophys. J.* 743, L14.
- Adrián-Martínez, S., Ageron, M., Aguilar, J.A., et al., 2012a. *J. Instrum.* 7, 8002.
- Adrián-Martínez, S., Samarai, I.A., Albert, A., et al., 2012b. *Astrophys. J.* 760, 53.
- Adrián-Martínez, S., Ageron, M., Aguilar, J.A., et al., 2013. *Astropart. Phys.* 42, 7.
- Ageron, M., et al., 2011. *Nucl. Instrum. Methods A* 656, 11.
- Agrawal, V., Gaisser, T.K., Lipari, P., Stanev, T., 1996. *Phys. Rev. D* 53, 1314.
- Aguilar, J.A., Albert, A., Ameli, F., et al., 2007. *Nucl. Instrum. Methods Phys. Res., Sect. A* 570, 107.
- Aguilar, J.A., Al Samarai, I., Albert, A., et al., 2011a. *Astropart. Phys.* 34, 539.
- Aguilar, J.A., et al., 2011b. *Phys. Lett. B* 696, 16.
- Amram, P., Anghinolfi, M., Anvar, S., et al., 2002. *Nucl. Instrum. Methods Phys. Res., Sect. A* 484, 369.
- Baerwald, P., Guetta, D., 2013. *Astrophys. J.* 773, 159.
- Belloni, T.M., 2010. In: Belloni, T. (Ed.), *Lecture Notes in Physics*, vol. 794. Springer-Verlag, Berlin, p. 53.
- Belloni, T., Motta, S., Muñoz-Darias, T., 2010. *Astron. Telegram* 2577.

⁵ This ratio is called K_{pe} in Zhang et al. (2010).

- Bowyer, S., Byram, E.T., Chubb, T.A., Friedman, H., 1965. *Science* 147, 394.
- Calvelo, D.E., Fender, R., Broderick, J., et al., 2010. *Astron. Telegram* 2699.
- Capitanio, F., Belloni, T., Del Santo, M., Ubertini, P., 2009. *Mon. Not. R. Astron. Soc.* 398, 1194.
- Carminati, G., Bazzotti, M., Margiotta, A., Spurio, M., 2008. *Comput. Phys. Commun.* 179, 915.
- Casella, P., Maccarone, T.J., O'Brien, K., et al., 2010. *Mon. Not. R. Astron. Soc.* 404, L21.
- Chen, Y.P., Zhang, S., Torres, D.F., et al., 2010. *Astron. Astrophys.* 522, A99.
- Corbel, S., Fender, R.P., Tzioumis, A.K., et al., 2002. *Science* 298, 196.
- Corbel, S., Kaaret, P., Fender, R.P., et al., 2005. *Astrophys. J.* 632, 504.
- Corbel, S., Tzioumis, T., Brocksopp, C., Fender, R., 2007. *Astron. Telegram* 1007.
- Díaz Trigo, M., Miller-Jones, J.C.A., Migliari, S., Broderick, J.W., Tzioumis, T., 2013. *Nature* 504, 260.
- Distefano, C., Guetta, D., Waxman, E., Levinson, A., 2002. *Astrophys. J.* 575, 378.
- Feldman, G.J., Cousins, R.D., 1998. *Phys. Rev. D* 57, 3873.
- Fender, R.P., Pooley, G.G., Durouchoux, P., Tilanus, R.P.J., Brocksopp, C., 2000. *Mon. Not. R. Astron. Soc.* 312, 853.
- Fender, R., Wu, K., Johnston, H., et al., 2004a. *Nature* 427, 222.
- Fender, R.P., Belloni, T.M., Gallo, E., 2004b. *Mon. Not. R. Astron. Soc.* 355, 1105.
- Fender, R.P., Stirling, A.M., Spencer, R.E., et al., 2006. *Mon. Not. R. Astron. Soc.* 369, 603.
- Fender, R.P., Homan, J., Belloni, T.M., 2009. *Mon. Not. R. Astron. Soc.* 396, 1370.
- Gallo, E., Corbel, S., Fender, R.P., Maccarone, T.J., Tzioumis, A.K., 2004. *Mon. Not. R. Astron. Soc.* 347, L52.
- Gallo, E., Fender, R., Kaiser, C., et al., 2005. *Nature* 436, 819.
- Gies, D.R., Bolton, C.T., 1986. *Astrophys. J.* 304, 371.
- Goss, W.M., Mebold, U., 1977. *Mon. Not. R. Astron. Soc.* 181, 255.
- Grinberg, V., Hell, N., Pottschmidt, K., et al., 2013. *Astron. Astrophys.* 554, A88.
- Heinz, S., 2006. *Astrophys. J.* 636, 316.
- Hynes, R.I., Steeghs, D., Casares, J., Charles, P.A., O'Brien, K., 2003. *Astrophys. J.* 583, L95.
- Jonker, P.G., Nelemans, G., 2004. *Mon. Not. R. Astron. Soc.* 354, 355.
- Jonker, P.G., Miller-Jones, J., Homan, J., et al., 2010. *Mon. Not. R. Astron. Soc.* 401, 1255.
- Kalemci, E., Tomsick, J.A., Yamaoka, K., Ueda, Y., 2007. *Astron. Telegram* 1348, and references therein.
- Kaluzienski, L.J., Holt, S.S., Boldt, E.A., Serlemitsos, P.J., 1976. *Astrophys. J.* 208, L71.
- Kennea, J.A., Capitanio, F., 2007. *Astron. Telegram* 1140.
- Levinson, A., Waxman, E., 2001. *Phys. Rev. Lett.* 87, 171101.
- Liu, Q.Z., van Paradijs, J., van den Heuvel, E.P.J., 2006. *Astron. Astrophys.* 455, 1165.
- Liu, Q.Z., van Paradijs, J., van den Heuvel, E.P.J., 2007. *Astron. Astrophys.* 469, 807.
- Marshall, H.L., Canizares, C.R., Schulz, N.S., 2002. *Astrophys. J.* 564, 941.
- McClintock, J.E., Remillard, R.A., Rupen, M.P., et al., 2009. *Astrophys. J.* 698, 1398.
- Migliari, S., Fender, R., Méndez, M., 2002. *Science* 297, 1673.
- Miller-Jones, J.C.A., Blundell, K.M., Rupen, M.P., et al., 2004. *Astrophys. J.* 600, 368.
- Miller-Jones, J.C.A., Moin, A., Tingay, S.J., et al., 2012a. *Mon. Not. R. Astron. Soc.* 419, L49.
- Miller-Jones, J.C.A., Sivakoff, G.R., Altamirano, D., et al., 2012b. *Mon. Not. R. Astron. Soc.* 421, 468.
- Mirabel, I.F., Rodríguez, L.F., 1994. *Nature* 371, 46.
- Moin, A., Reynolds, C., Miller-Jones, J.C.A., et al., 2011. *Mon. Not. R. Astron. Soc.* 414, 3551.
- Motta, S., Belloni, T., Homan, J., 2009. *Mon. Not. R. Astron. Soc.* 400, 1603.
- Motta, S., Belloni, T., Muñoz-Darias, T., Homan, J., 2010. *Astron. Telegram* 2593.
- Murdin, P., Jauncey, D.L., Lerche, I., et al., 1980. *Astron. Astrophys.* 87, 292.
- Nakahira, S., et al., 2010. *Astron. Telegram* 2774.
- Pandey, M., Manchanda, R.K., Rao, A.P., Durouchoux, P., Ishwara-Chandra, C.H., 2006. *Astron. Astrophys.* 446, 471.
- Parsignault, D.R., Gursky, H., Kellogg, E.M., et al., 1972. *Nature* 239, 123.
- Predehl, P., Burwitz, V., Paerels, F., Trümper, J., 2000. *Astron. Astrophys.* 357, L25.
- Romero, G.E., Torres, D.F., Kaufman Bernadó, M.M., Mirabel, I.F., 2003. *Astron. Astrophys.* 410, L1.
- Sahakyan, N., Piano, G., Tavani, M., 2014. *Astrophys. J.* 780, 29.
- Shidatsu, M., Ueda, Y., Tazaki, F., et al., 2011. *Publ. Astron. Soc. Jpn.* 63, 785.
- Steiner, J.F., McClintock, J.E., Reid, M.J., 2012. *Astrophys. J.* 745, L7.
- Stirling, A.M., Spencer, R.E., de la Force, C.J., 2001. *Mon. Not. R. Astron. Soc.* 327, 1273.
- Tavani, M., et al., 2009. *Nature* 462, 620.
- van Kerkwijk, M.H., Charles, P.A., Geballe, T.R., et al., 1992. *Nature* 355, 703.
- Webster, B.L., Murdin, P., 1972. *Nature* 235, 37.
- Williams, P.K.G., Tomsick, J.A., Bodaghee, A., et al., 2011. *Astrophys. J.* 733, L20.
- Xiang, J., Lee, J.C., Nowak, M.A., Wilms, J., 2011. *Astrophys. J.* 738, 78.
- Yamaoka, K., et al., 2009. *Astron. Telegram* 2364.
- Zdziarski, A.A., Gierliński, M., Mikołajewska, J., et al., 2004. *Mon. Not. R. Astron. Soc.* 351, 791.
- Zhang, J.F., Feng, Y.G., Lei, M.C., Tang, Y.Y., Tian, Y.P., 2010. *Mon. Not. R. Astron. Soc.* 407, 2468.